Available online at www.sciencedirect.com
SCIENCE DIRECT®
Physica A 317 (2003) 411–431
PHYSICA A
www.elsevier.com/locate/physa

Chaotic magnetic field lines in tokamaks with ergodic limiters

Jefferson S.E. Portela[a], Ricardo L. Viana[a,*], Iberê L. Caldas[b]

[a] *Departamento de Física, Universidade Federal do Paraná, C.P. 19081, 81531-990 Curitiba, PR, Brazil*

[b] *Instituto de Física, Universidade de São Paulo, C.P. 66318, 05315-970, São Paulo, Brazil*

Received 24 May 2002; received in revised form 12 July 2002

Abstract

We consider a symplectic map for magnetic field lines in a tokamak with an ergodic limiter, whose function is to generate a perturbing magnetic field which causes the formation of chaotic field lines in the vicinity of the tokamak inner wall. We analyze numerically the onset of global chaos due to the interaction of adjacent magnetic islands, the size of the chaotic region, and investigate anomalous diffusion and loss of field lines due to their collisions with the tokamak wall.

Keywords: Lagrangean chaos; Tokamaks; Magnetic field lines

1. Introduction

Tokamaks are toroidal systems in which plasmas are generated by the ohmic heating of a filling gas and confined by externally applied magnetic fields. The magnetic field lines have helical shape and lie on magnetic flux surfaces with topology of nested tori [1]. An important problem in the obtention of plasma discharges in tokamaks is the control of plasma contamination by impurities released from the inner wall by surface processes [2]. In order to control these plasma–wall interactions, there has been proposed the creation of a region of chaotic field lines in the periphery of the tokamak vessel [3–5]. Chaotic magnetic field lines are taken here from a Lagrangian perspective, since the configurations we dealt with in this paper are strictly magnetostatic. Sensitive dependence to initial conditions, in this sense, means that two field line points, very

* Corresponding author.
E-mail address: viana@fisica.ufpr.br (R.L. Viana).

0378-4371/03/$ - see front matter
PII: S0378-4371(02)01351-1

close from each other at some spatial position, will evolve through a large number of revolutions around the torus such that the distance between them increases at a positive exponential rate [6,7].

The generation of chaotic magnetic field lines in the outer tokamak region can be done by breaking the spatial symmetry of the configuration, through the destruction of some carefully chosen magnetic surfaces in this region. The ergodic magnetic limiter (EML) is a device designed to generate external magnetic fields which interact with the equilibrium tokamak field and cause a selective destruction of magnetic surfaces [3–5]. The spatial behavior of the magnetic field lines can be studied by means of a Poincaré map, considering the intersections of the field lines with a fixed surface of section.

The use of mappings to study field line dynamics is a common tool in plasma physics. Recent works include the study of ergodic divertors [8,9] and general symmetry-breaking perturbations [10]. The case of a EML was first treated by Martin and Taylor [11], who have derived analytically a two-dimensional field line map in a rectangular geometry, appropriate to describe the region immediately near the tokamak wall. It has been subsequently improved with the addition of toroidal corrections and parameters describing the equilibrium and perturbed magnetic fields [12–14]. Recently, it has been proposed a symplectic map for a EML considering a toroidal geometry, and using magnetic fields consistent with a MHD equilibrium theory [15]. Magnetic field line mappings present an advantage due to the higher computation speed of their iteration, when compared with the numerical integration of the field line differential equations. This difference is relevant if long-term behavior of field lines is being considered, as in numerical studies of anomalous diffusion, field line losses due to collisions with the tokamak wall [16], bifurcations [17], and fractal exit basin boundaries [18].

The mapping of Ref. [11] is a useful tool to investigate the magnetic field line behavior due to arbitrary symmetry-breaking perturbations in tokamaks. It is exactly area-preserving, which is necessary in order to the map be consistent with magnetic flux conservation. Moreover, it exhibits resonances with unequal amplitudes, a situation often found in physical applications where the perturbation is localized in space. The Chirikov–Taylor standard map [19], on the other hand, which is commonly used to this purpose [20], has resonances with equal widths and hence it is not suitable to model the effect of a EML. Moreover, the double periodicity present in the standard map leads to the so-called accelerator models, which are not usually found in field line mappings [21].

The main purpose of this paper is to revisit the model of Ref. [11] so as to compare some known analytical approximate results with numerical estimates for periodic orbits, island positions, the onset of global chaos, and the size of the chaotic region. In particular we describe a numerical procedure to find accurately the barrier transition to global chaos, and investigate the validity of the Chirikov overlapping criterion [19] for this situation. Another issue to be treated is the field line anomalous diffusion in the mainly chaotic tokamak edge, and the loss of chaotic field lines due to their collisions with the tokamak wall.

This paper is organized as follows: in Section 2 we outline the derivation of the symplectic map for a EML. Section 3 is devoted to an analysis of many properties of

the map, such as its fixed points and periodic islands. Section 4 focuses on the barrier transition to global chaos, and Section 5 treats diffusion and loss in the chaotic region near the wall. Our conclusions are left to the last section.

2. Symplectic map for field lines

The basic toroidal geometry of a tokamak is depicted in Fig. 1. The major axis is parametrized by the Z coordinate, and we set the radius R with respect to it, in a cylindrical coordinate system, Φ being the corresponding azimuthal angle. The minor axis of the tokamak is located at $R = R_0$, where R_0 is the major radius of the torus, and the vessel wall is located at a distance b (minor radius) from the minor axis. We define an aspect ratio $A = R_0/b$ for the torus such that, if A is large enough, we can neglect the toroidal curvature and approximate the tokamak by a periodic cylinder of length $2\pi R_0$. The minor axis can now be used to define a second cylindrical coordinate system with coordinates r, θ and $z = R_0\Phi$, such that the tokamak wall is located at $r = b$. The variables θ and Φ are usually quoted as the poloidal and toroidal angles, respectively. The relations between these coordinate systems are $R = R_0 + r\cos\theta$, and $Z = r\sin\theta$.

In this paper, we are concerned with the behavior immediately near the tokamak wall, and in this case even the poloidal curvature may be neglected in a first approximation, such that we can use a rectangular coordinate system (Fig. 2) $x = b\theta$, and $y = b - r$, where $0 < x < 2\pi b$ represents the rectified arc along the tokamak wall, and y is the radial distance from it [11]. Points with $y > 0$ (< 0) are located inside (outside) the torus.

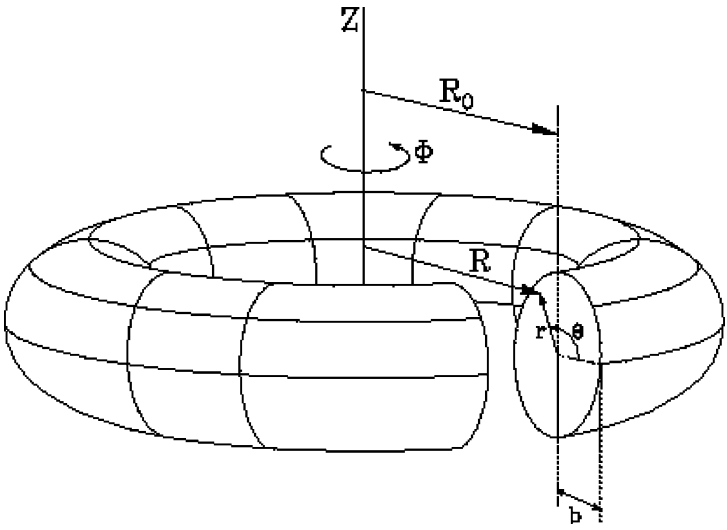

Fig. 1. Schematic view of a tokamak showing the coordinate systems used in this paper.

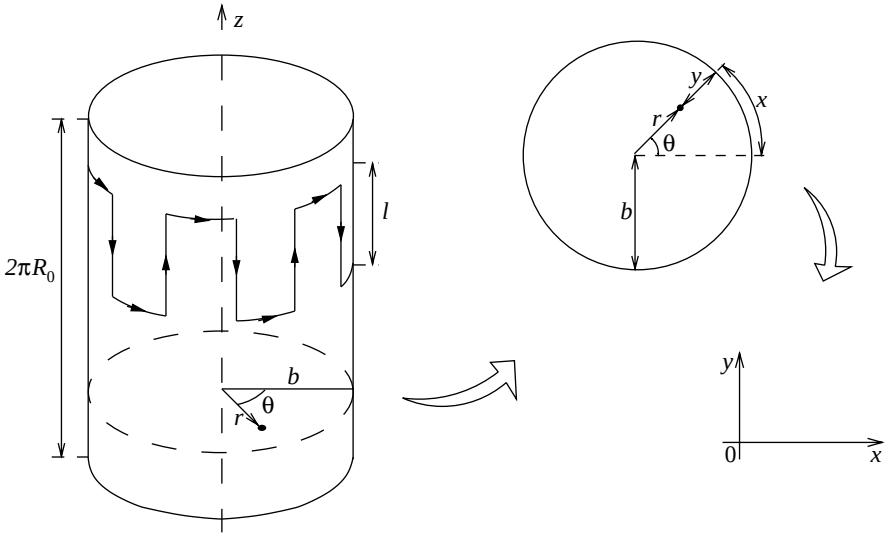

Fig. 2. Schematic view of the tokamak in the periodic cylinder approximation and the coordinates used in the rectangular geometry.

A tokamak confines a plasma by the combined action of two basic magnetic fields: (i) a toroidal field $\mathbf{B}_T$ along the $\hat{e}_\Phi$ direction, generated by coils wound around the torus; (ii) a poloidal field $\mathbf{B}_P$ along the $\hat{e}_\theta$ direction, generated by the plasma column itself [1]. The superposition $\mathbf{B}_0 = \mathbf{B}_T + \mathbf{B}_P$ is called the equilibrium magnetic field and the resulting magnetic field lines have a helical shape, their pitch being described by the *safety factor* $q(r) = \mathrm{d}\Phi/\mathrm{d}\theta$.

The magnetic field line equations, viz. $\mathbf{B}_0 \times \mathbf{dr} = \mathbf{0}$, where $\mathbf{B}_0 = (B_{0x}, B_{0y}, B_{0z})$, are written in rectangular coordinates as

$$\frac{\mathrm{d}x}{B_{0x}} = \frac{\mathrm{d}y}{B_{0y}} = \frac{\mathrm{d}z}{B_{0z}} \,. \tag{1}$$

In the periodic cylinder approximation, we assume that the toroidal equilibrium field is uniform $B_{0z} \equiv B_0$.

Ideal MHD theory predicts that the equilibrium magnetic field lines, in the absence of symmetry-breaking perturbations, lie on constant-pressure *flux surfaces* with a toroidal shape [6]. In the cylindrical approximation a flux surface is characterized by $q(r) = constant$. In particular, $q_b = q(r = b)$ is the safety factor at the tokamak wall, and we define

$$\alpha = \frac{2\pi b}{q_b} \,. \tag{2}$$

In typical experiments the safety factor radial profile is monotonically increasing from $q(0) \approx 1$, at the minor axis, to $q_b \approx 5$ [1], with a *magnetic shear*

$$s = \frac{2\pi b}{q_b^2} \frac{\mathrm{d}q}{\mathrm{d}r}\bigg|_{r=b} \,. \tag{3}$$

Since we are interested in the immediate vicinity of the wall, we can expand the safety factor in powers of $y = b - r$

$$q(y) = \frac{b}{R_0}\frac{\mathrm{d}z}{\mathrm{d}x} = 2\pi b[\alpha + sy + o(y^2)]^{-1} \tag{4}$$

such that the magnetic field line equations (1) read

$$\frac{\mathrm{d}x}{\mathrm{d}z} = \frac{1}{2\pi R_0}[\alpha + sy + o(y^2)]\,, \tag{5}$$

$$\frac{\mathrm{d}y}{\mathrm{d}z} = 0\,. \tag{6}$$

The EML configuration we consider in this paper consists on a grid-shaped ring of width ℓ (see Fig. 2) mounted externally to the torus (neglecting the thickness of the vessel wall), and with two kinds of segments: toroidally oriented (TO) and poloidally oriented (PO) ones [11]. There are m pairs of TO segments, equally spaced along the poloidal direction, with adjacent segments conducting a current I in opposite senses. Only the TO segments are relevant to the perturbing field of the EML [22]. In terms of the rectangular geometry considered here, the TO segments are on the xy-plane, $\pi b/m$ apart from each other. For low-beta plasmas we deal with a vacuum field, for which $\mathbf{B}_1 = \nabla\phi_M$, in terms of a scalar potential satisfying Laplace's equation, for which proper boundary conditions are imposed on the $y = 0$ plane, where the surface density current due to the EML ring is [22]

$$\mathbf{j}(x) = \hat{e}_z \frac{I}{b}\sum_{k=1}^{2m}(-1)^k \delta\left(x - \frac{k\pi b}{m}\right) \tag{7}$$

and we have assumed that the TO segments are infinitely long.

Expanding the periodic delta function in (7) in a series of sinusoidal harmonics, it turns out that the magnetic field components of very long TO segments are given by [22]

$$B_{1x}^{(a)}(x,y) = -\frac{\mu_0 mI}{b\pi}\exp\left(-\frac{my}{b}\right)\cos\left(\frac{mx}{b}\right)\,, \tag{8}$$

$$B_{1y}^{(a)}(x,y) = +\frac{\mu_0 mI}{b\pi}\exp\left(-\frac{my}{b}\right)\sin\left(\frac{mx}{b}\right)\,, \tag{9}$$

$$B_{1z}^{(a)}(x,y) = 0\,. \tag{10}$$

However, the EML ring has a finite length ℓ and, neglecting border effects, we make the crude approximation that inside the limiter (i.e., when $0 \leqslant z \leqslant \ell$) the EML field is given by (8)–(10), whereas outside it only the equilibrium magnetic field is present and the field lines satisfy Eqs. (5) and (6).

The EML map is defined through a Poincaré surface of section at the $\Phi = 0$, such that x_n and y_n are coordinates of the nth piercing of a field line on this plane. Since the independent (or time-like) variable in the magnetic field line equations is the z-variable, and since there is a periodicity of $T \equiv 2\pi R_0$ in this direction, we can regard the process

as a stroboscopic, or "time-T" map of the flow given by (1). In order to evaluate the kick suffered by a field line due to the EML, we define auxiliary variables x_n^*, y_n^* as the coordinates sampled at the EML edge $z=\ell$. If the limiter length ℓ is small enough, we can approximately integrate the differential equations by Euler's method, evaluating the EML field at $z=0$ and extrapolating the result to the other edge ($z=\ell$). There results [11]

$$x_n^* = x_n - \frac{bp}{m}\exp\left(-\frac{my_n}{b}\right)\cos\left(\frac{mx_n}{b}\right) , \tag{11}$$

$$y_n^* = y_n + \frac{b}{m}\ln\left\{\cos\left[\frac{mx_n}{b} - p\exp\left(-\frac{my_n}{b}\right)\cos\left(\frac{mx_n}{b}\right)\right]\right\} - \frac{b}{m}\ln\cos\left(\frac{mx_n}{b}\right) , \tag{12}$$

where

$$p = \frac{\mu_0 \ell m^2 I}{B_0 b^2 \pi} \tag{13}$$

represents the strength of the EML action, proportional to the limiter current.

Outside the limiter ($\ell < z < 2\pi R_0$) the field line equations (5)–(6) can be exactly integrated to give the coordinates of the $(n+1)$th mapping point on the Poincaré surface of section $z=0$

$$x_{n+1} = x_n^* + \alpha + sy_n^* , \tag{14}$$

$$y_{n+1} = y_n^* \tag{15}$$

meaning that, in absence of perturbation, the field line intersections with the plane are constrained to lie on straight lines for which y is constant.

It is useful to define non-dimensional variables

$$x' \equiv \frac{mx}{b} , \tag{16}$$

$$y' \equiv \frac{m}{b}\left(y + \frac{\alpha}{s}\right) , \tag{17}$$

such that the new origin ($y'=0$) corresponds to the point $y_0=-\alpha/s$, for which $x_n^*=x_{n+1}$. Since $0 \leqslant x' < 2\pi$, x is defined modulo $2\pi b/m$, and the safety factor at y_0 is then m/K, where K is an integer. In terms of these normalized variables, the pairs of difference equations (11)–(12) and (14)–(15) can be written as the composition of two mappings $T = T_2 \circ T_1$, where T_2 corresponds to the limiter action

$$x_n'^* = x_n' - pe^{-y_n'}\cos x_n' , \tag{18}$$

$$y_n'^* = y_n' + \ln[\cos(x_n' - pe^{-y_n'}\cos x_n')] - \ln(\cos x_n') \tag{19}$$

and T_1 to the field line twist on a flux surface

$$x_{n+1}' = x_n'^* + sy_n'^* , \tag{20}$$

$$y_{n+1}' = y_n'^* . \tag{21}$$

3. Properties of the EML map

For later convenience, let us write the map T in a more compact form, dropping the primes on the variables for simplicity

$$x_{n+1} = x_n + s y_n + g(x_n, y_n)\,, \tag{22}$$

$$y_{n+1} = y_n + h(x_n, y_n)\,, \tag{23}$$

where

$$h(x, y) = \ln\left[\frac{\cos\left(x - p\mathrm{e}^{-y}\cos x\right)}{\cos x}\right]\,, \tag{24}$$

$$g(x, y) = -p\,\mathrm{e}^{-y}\cos x + sh(x, y)\,. \tag{25}$$

The map (22)–(23) is *exactly* area-preserving, for its Jacobian is equal to the unity, in spite of the number of approximations we made in the derivation of the map equations. Incidentally, if we expand the functions defined above in powers of the diffuser strength p, it turns out that the Jacobian is now $1 + o(p^2)$.

Eqs. (22) and (23) define a Hamiltonian mapping, in the sense that (x, y) may be regarded as canonically conjugated variables, whereas the ignorable coordinate z (in the symmetric case) plays the role of time. In this case, the magnetic field line equations (1) can be written as Hamilton equations [7,23,24]

$$\frac{\mathrm{d}x}{\mathrm{d}z} = \frac{\partial H}{\partial y}\,, \tag{26}$$

$$\frac{\mathrm{d}y}{\mathrm{d}z} = -\frac{\partial H}{\partial x}\,, \tag{27}$$

in which H is the field line Hamiltonian. For the equilibrium field $\mathbf{B}_0$, H depends only on the radial variable, what characterizes an integrable system (in the sense of having one constant of motion), such that (y,x) are action and angle variables, respectively [21]. Considering Eq. (1), for example, the integrable Hamiltonian is $H_0(y)=B_{0x}(y)/B_0$.

The presence of an EML breaks the z-symmetry of the system, which becomes non-integrable. For weak limiter currents (in comparison with the plasma current) the limiter strength p is accordingly small and we can treat the problem as a near-integrable one. We can thus write the EML map in the form of a perturbed twist mapping [21]

$$x_{n+1} = x_n + 2\pi\mathscr{A}(y_n) + g(x_n, y_n)\,, \tag{28}$$

$$y_{n+1} = y_n + h(x_n, y_n)\,, \tag{29}$$

where

$$\mathscr{A}(y) = \frac{1}{2\pi}\,s y \tag{30}$$

is called the rotation number, and the functions $g(x, y)$ and $h(x, y)$ are related to derivatives of the perturbation Hamiltonian $H_1(x, y, z)$, provided we write the z-dependence

of the latter as a periodic sequence of delta functions [25]

$$H_1(x,y,z) = \sum_{j=-\infty}^{+\infty} \tilde{H}_1(x,y)\delta(z - 2\pi R_0 j)\,, \tag{31}$$

such that the near-integrable system has a total Hamiltonian

$$H(x,y,z) = H_0(y) + H_1(x,y,z)\,, \tag{32}$$

where $|H_1| \ll |H_0|$.

The fixed points of the EML map (22)–(23) are the solutions of the transcendental equations

$$x^* = \pi n + \frac{p}{2}\,\mathrm{e}^{-y^*}\cos x^*\,, \tag{33}$$

$$y^* = \frac{2\pi n}{s} + \frac{p}{s}\,\mathrm{e}^{-y^*}\cos x^*\,, \tag{34}$$

where n is a positive integer, which comes from the fact that x is defined *modulo* 2π, i.e., $x = x \pm 2\pi n$. We can use an approximate procedure, if p is small enough, and insert the right-hand side of Eq. (33) back into the cosine, and expand the result in powers of p. Just one iteration is sufficient to yield results up to quadratic terms in p:

$$x_1^* = +\frac{p}{2}\exp\left(-\frac{2\pi n}{s}\right) + o(p^2)\,, \tag{35}$$

$$x_2^* = \pi - \frac{p}{2}\exp\left(-\frac{2\pi n}{s}\right) + o(p^2)\,. \tag{36}$$

Substituting these results into (34) and expanding again in powers of p there results [11]

$$y^* = \frac{2\pi n}{s} - \frac{p}{s}\exp\left(-\frac{2\pi n}{s}\right) + o(p^2)\,. \tag{37}$$

We have developed a numerical algorithm to find the location of the fixed point x_2^*, using the above results as an initial step. The map trajectories in the vicinity of the fixed point (x_2^*, y^*) are ellipses encircling it, and since Eqs. (36)–(37) do not give the exact location of the fixed points, if we use them as initial conditions, the resulting map trajectories in the phase plane (x, y) will be closed orbits of elliptic shape and very small size. A numerical refinement of the fixed point location can be obtained by averaging the x and y values of all points of this elliptic orbit, yielding an improved estimate for (x_2^*, y^*). The procedure can be repeated until we achieve the desired accuracy.

Fig. 3 shows the radial location of the fixed point (x_2^*, y^*) for $n = 0$, and using: (i) the approximate analytical result of Eq. (37); (ii) a numerical solution of the transcendental equations (33)–(34); and (iii) the refinement algorithm described in the previous paragraph. Whereas the latter two results always seem to coincide, it turns out that the analytical result from (37) holds only for small p (Fig. 3a), what could be already expected due to the power expansions we have used to derive this result.

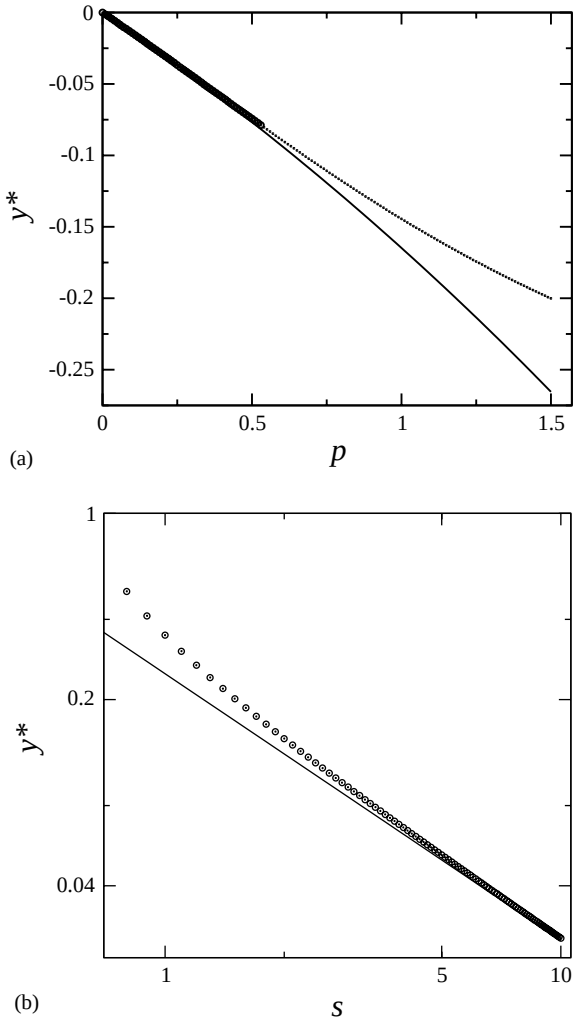

Fig. 3. Radial location of the elliptic fixed points of the EML map (22)–(23) for $n = 0$, as a function of (a) the limiter strength; and (b) the magnetic shear. Dots: numerical solution of Eq. (34); circles: refinement algorithm; full lines: approximate analytical result from Eq. (37).

In Fig. 3b we perform a similar comparison for varying magnetic shear, and show that the analytical result is satisfactory for high shear ($s \gtrsim 5$).

To study the linear stability properties of such fixed points, we can compute either the eigenvalues of the Jacobian matrix $\mathbf{J}$ of map (22)–(23) or the Greene residue [26]

$$R = \frac{1}{4}(2 - \mathrm{Tr}\,\mathbf{J})\,. \tag{38}$$

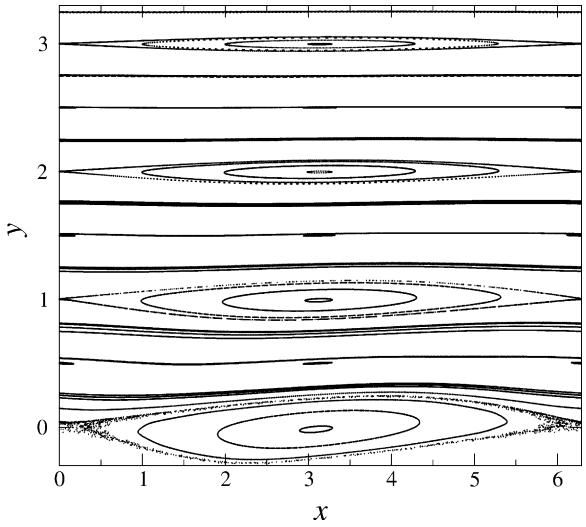

Fig. 4. Phase portrait for the EML map for $p = 0.1$ and $s = 2\pi$.

If $0 < R < 1$ the eigenvalues of $\mathbf{J}$ are pure imaginary and complex conjugates of each other, so that (x^*, y^*) is an elliptic point, or a center. Otherwise, the eigenvalues are real numbers, and the fixed point is a (hyperbolic) saddle point, hence linearly unstable. The residues for the fixed points (35) and (36) are, respectively, given by

$$R(x^*_{1,2}, y^*) = \mp\frac{1}{4}\, ps \exp\left(-\frac{2\pi n}{s}\right) + o(p^2) \tag{39}$$

and since both p and s are assumed to be positive, it turns out that $R(x^*_1) < 0$, hence x^*_1 is a hyperbolic point. Similarly, x^*_2 will be an elliptic point if $ps\exp(-2\pi n/s) < 4$, a condition fulfilled by most numerical applications we deal with in this paper.

In Fig. 4 we show a large number of orbits obtained for the EML map in a large-shear and low-strength situation, and for which the small-p expansions we used are in agreement with numerical results (see Fig. 3). Primary periodic islands encircle the elliptic fixed points $x^*_2 \approx \pi$ and $y^* \approx 0, 1, 2, \ldots$. From Eq. (16), since y is a reduced variable, a single primary island in the phase portraits corresponds to a chain of m islands in the tokamak. These islands have each a structure topologically similar to that of a non-linear pendulum, but since there is a symmetry-breaking perturbation, the island separatrices no longer cross themselves at the hyperbolic points ($x^*_1 \approx 0$), as would occur with a pendulum. They have instead a rather involved behavior characterized by a local chaotic layer at the island border [21].

4. Transition to global chaos

The primary islands shown in Fig. 4 are centered at the elliptic fixed points of the EML map (22)–(23), $y^*_n = 2\pi n/s + o(p)$, for $n = 0, 1, 2, \ldots$, and result from resonances

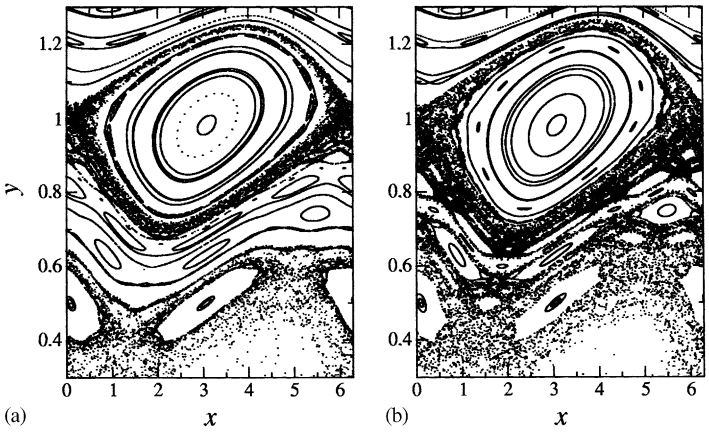

Fig. 5. Phase portrait for the EML map for $s = 2\pi$ and (a) $p = 0.29$ and (b) $p = 0.32$; respectively, after and before the barrier transition to global chaos.

between the harmonics of the EML field and the equilibrium magnetic field. In terms of the corresponding perturbed twist map, the rotation number at the fixed point is, from Eq. (30), $\mathscr{A}(y_n^*) = n + o(p)$. Hence we label the primary islands as $n = 0, 1, 2, \ldots$, in increasing order of distance from the tokamak wall.

In the absence of perturbations the twist map (28)–(29) results in $(\Delta x)_n = x_{n+1} - x_n = 2\pi\mathscr{A}(y_n)$. The island centers represent exact resonances, for the unperturbed field lines at those positions would close on themselves after k complete turns around the z-direction. From (4) the safety factor at a resonance centered at y_n^* is

$$q(y_n^*) = \frac{b}{R_0}\,\frac{k}{2\pi}\,\frac{2\pi R_0}{\mathscr{A}(y_n^*)} = b\left(\frac{k}{n}\right) . \tag{40}$$

If both k and n are co-prime integers, it turns out that the safety factor at an island center is proportional to a rational number k/n [24]. We have mentioned in Section 2 that the safety factor can be used to label the equilibrium flux surfaces on which unperturbed magnetic field lines lie. Assuming that the safety factor depends monotonically on y, there results that each flux surface has a different safety factor. A rational (irrational) flux surface is thus characterized by a rational (irrational) safety factor [7]. In quasi-periodic orbits, a field line never closes on itself, rather filling densely an irrational flux surface, which appear as invariant curves between adjacent primary islands, in the phase portraits. These surfaces survive to a perturbation weak enough, according to the KAM theorem [27].

As the perturbation strength p increases, the phase portrait begins to show, besides the KAM tori, also higher-order islands, which are structured around periodic orbits of the symplectic map with higher integer periods (Fig. 5). In addition, thin area-filling regions are present in the neighborhood of the island borders, corresponding to dense chaotic orbits [21]. If p builds up further, the region between two adjacent islands becomes progressively engulfed by the chaotic regions surrounding each island border.

However, as long as we have KAM tori between these islands, the chaotic excursion of a single orbit is limited to a distance of the order of the island width.

Using a perturbative technique (global removal of resonances), Martin and Taylor [11] have found an approximate invariant which can be used to predict the half-width of an island centered at $y_n^* \approx 2\pi n/s$

$$\Delta y_n = 2\sqrt{\frac{p}{s}}\exp\left(-\frac{\pi n}{s}\right) + o(p) \tag{41}$$

showing that the island width increases with the square root of the limiter strength and decreases exponentially with the island position, as we can observe in the phase portraits of Fig. 4.

On the other hand, the separation between two adjacent islands does not depend on n, since

$$\delta y = y_{n+1}^* - y_n^* = \frac{2\pi}{s} + \frac{p}{s}\exp\left(-\frac{2\pi}{s}\right) \tag{42}$$

and the consequence is that, as p increases, the regions between adjacent islands are altered in quantitatively different ways. For example, for the same value of p, the region between the $n = 0$ and 1 primary islands is more affected by the presence of chaotic field than the region between the $n = 1$ and 2 ones. This is due to the EML action being mainly near the tokamak wall.

The chaotic excursion of a field line can be substantially increased if two adjacent islands fuse their locally chaotic regions, producing global chaos. Since this demands the destruction of all KAM tori between two interacting islands, we expect a barrier transition: after the transition, the chaotic radial excursion of a field line suddenly increases to a distance nearly twice as large. The Chirikov overlapping criterion [19] prescribes the onset of global chaos when the borders of two adjacent island touch themselves. Defining a stochasticity parameter

$$S_{n,n+1} = \frac{\Delta y_{n+1} + \Delta y_n}{\delta y} \tag{43}$$

such a barrier transition for global chaos occurs when S reaches the critical value $S_c = 1$. However, the latter value turns to be too large, when compared with numerical results [26]. In practice, the barrier transition occurs *before* $S_c = 1$, basically for two reasons: (i) there are no sharp separatrices at the island borders, so we have to take into account the widths of the locally chaotic regions; (ii) there exist higher-order islands between adjacent primary resonances, and they have their own chaotic regions, contributing to the formation of a connected chaotic web [21].

The barrier transition has been extensively studied for the standard map [19]

$$x_{n+1} = x_n + y_{n+1}\,, \tag{44}$$

$$y_{n+1} = y_n + K\sin x_n \tag{45}$$

for which all primary islands have equal widths $\Delta y_n = 2\sqrt{K}$, and are separated by a fixed distance $\delta y_n = 2\pi$, such that the corresponding stochasticity parameter is $S = 2\sqrt{K}/\pi$. Careful numerical experiments [26] have determined that the barrier transition

occurs at $K_c \approx 0.9716$. This corresponds to a last KAM torus between two primary island with irrational rotation number equal to the golden mean $(\sqrt{5}-1)/2$ [28]. If we continue to use the stochasticity parameter (43) to describe the barrier transition, this numerical result amounts to a critical stochasticity parameter $S_c \approx \frac{2}{3}$, the so-called "two-thirds rule", which is an empirical correction to the Chirikov criterion [21]. Notice, however, that more sophisticated methods to predict a barrier transition are available, as the Doveil-Escande renormalization criterion [28], and the Greene residue technique [26].

In contrast with the standard map, the primary islands of the EML map have different widths according to their positions. Since only those islands with $n = 0$ and 1 have widths large enough to yield a sizeable chaotic region for p-values of practical interest, we consider just their interaction, and compute the corresponding stochasticity parameter. Substituting Eqs. (41) and (42) into (43), it reads

$$S_{0,1}(p,s) = \frac{1}{\pi}\sqrt{ps}(1+\mathrm{e}^{-\pi/s}) + o(p^{3/2}) \,. \tag{46}$$

We estimate the limiter strength threshold, p_c, by imposing that $S_{0,1}(p_c) = S_c$, what results in

$$p_c(S_c,s) = \frac{\pi^2}{s} S_c^2 (1+\mathrm{e}^{-\pi/s})^{-2} \,. \tag{47}$$

Let us consider the phase portraits depicted in Fig. 5. The two panels represent situations just after and before the barrier transition, which occurs for an estimated perturbation strength of $p_c \approx 0.29$. On the other hand, applying the two-thirds rule ($S_c = \frac{2}{3}$) in (47), there results a value $p_c = 0.27$, which represents an error less than 7% of the numerically observed value, and it is far better than the value (0.61) predicted for a simple touching of separatrices ($S_c = 1$). The numerical results we have obtained for p_c indicate that the necessary critical value for the stochasticity parameter must be about 0.69. We also remark that, since the interacting islands have unequal widths, at the barrier transition the last KAM torus to be broken between the primary islands is no longer the "golden torus". The successful application of the two-thirds rule in this case, even with islands of unequal widths, was already noted in Ref. [25].

In order to verify the theoretical prediction given by the modified Chirikov criterion (47) for the onset of global chaos, we have used a numerical procedure based on the fact that points of a chaotic orbit near a $n = 0$ island will eventually have negative y-values. The critical p_c will be the least value of p for which the points of a chaotic orbit belong simultaneously to the chaotic regions near both the $n = 0$ and 1 islands. We start with a rough estimate for p_c, as given for example by Eq. (47) and the two-thirds rule, and set p to be slightly less than this value. Next we use Eq. (37) to set up an initial condition at the hyperbolic fixed point for $n = 1$. This initial condition is certainly in the chaotic region near the $n = 1$ island, and we generate a long chaotic orbit iterating the map 500,000 times. If these points do not have negative y-values they much probably do not belong to the chaotic region near the $n = 0$ island, such that the barrier transition has not occurred yet. Next we increment p by a small amount, say 5×10^{-4}, and repeat this procedure until we detect negative y-values, what indicates that the barrier transition has been crossed. In this case we set p_c as the arithmetic mean

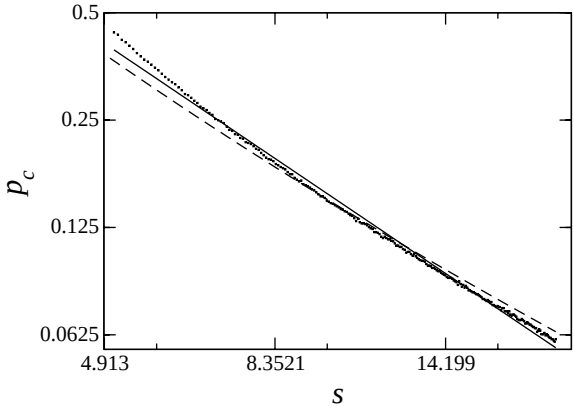

Fig. 6. Critical value of the limiter strength p necessary to the barrier transition leading to global chaos, as a function of the magnetic shear s. Full line: least-squares fit; dashed line: theoretical prediction from 2/3-rule.

between the two last p-values. In Fig. 6 we present results for p_c *versus* the magnetic shear. The points are obtained through the numerical procedure just described; the full line is a least-squares power-law fit $p_c(s) \sim s^{-\sigma}$, where $\sigma \approx 1.4$; and the dashed line is the result from Eq. (47) with $S_c = 2/3$, illustrating the good agreement between the two-thirds rule and the numerical results, for a wide range of magnetic shear values.

5. Chaotic field line diffusion and loss

The main goal of an ergodic limiter is to create a region of chaotic magnetic field lines near the tokamak wall. However, this has to be done in a controlled way so as not to destroy the plasma core. We thus have to constrain the width of the chaotic region such that it should contain the vacuum layer between the plasma and the inner tokamak wall, as well as some of the outer portion of the plasma column, but leaving a number of undestructed flux surfaces to confine a representative amount of plasma.

Let $y = A$ be an upper bound for the chaotic region, and it does not correspond necessarily to some KAM torus, since the latter typically presents some distortion in order to accommodate the neighboring pendular-shaped islands. Hence we may take $y = A$ as the poloidally averaged radius of the points belonging to this first KAM torus. Since the EML map (22)–(23) is invariant under the transformations [11]

$$y \to y + \frac{2\pi n}{s}\,, \tag{48}$$

$$p \to p \exp\left(\frac{2\pi n}{s}\right), \tag{49}$$

if $\ln p$ is increased by $2\pi/s$, the boundary of the chaotic region is likewise displaced by $2\pi/s$. Hence, the ratio between these two variations is equal to unity, or $\mathrm{d}A/\mathrm{d}(\ln p) = 1$

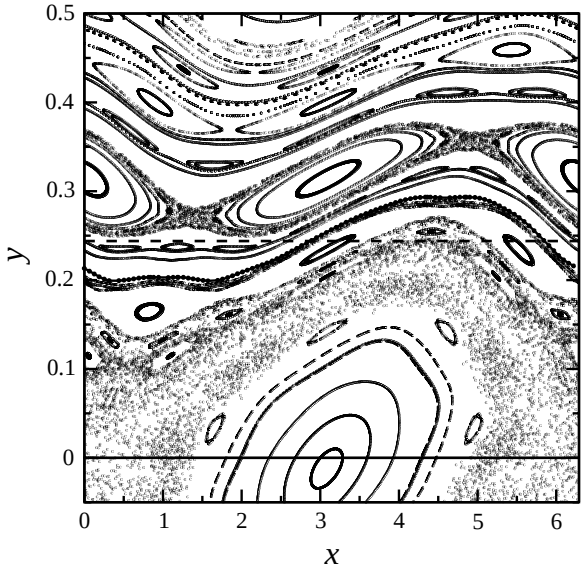

Fig. 7. Phase portrait for the EML map for $p = 0.1$ and $s = 10$. The full line indicates the tokamak wall, whereas the dashed line indicates the rough boundary of the chaotic region. The dotted line approximates the first KAM torus bounding the chaotic region.

which, by integration, gives

$$A(p,s) = \ln p + g(s)\,, \tag{50}$$

where $g(s)$ is an arbitrary function of the magnetic shear. Martin and Taylor [11] have estimated that, for typical tokamak parameters,

$$g(s) = \ln s + 0.03\,. \tag{51}$$

We can numerically estimate the width of the chaotic region by considering a phase portrait like that depicted in Fig. 7. The chaotic boundary, indicated by a dashed line in Fig. 7, is taken to be the average y-value of the first KAM torus, counted from the tokamak wall. The first KAM torus is represented by a dotted line in Fig. 7. We compare in Fig. 8 the prediction of Eq. (51) with the numerically determined values of A, by varying p (Fig. 8a) and s (Fig. 8b). The agreement is good as long as we have the correct trend for the averaged value, the oscillations around it being a result of the mentioned distortion of the KAM tori near islands' borders. In particular, this agreement is better for higher shear. It should be noted in both figures that each jump suffered by A, as either p or s are increased, corresponds to a different barrier transition, which means that different adjacent pairs of islands (namely those with n and $n+1$) are progressively fusing their locally chaotic layers. These layers, on their turn, add to the already existing global chaotic region.

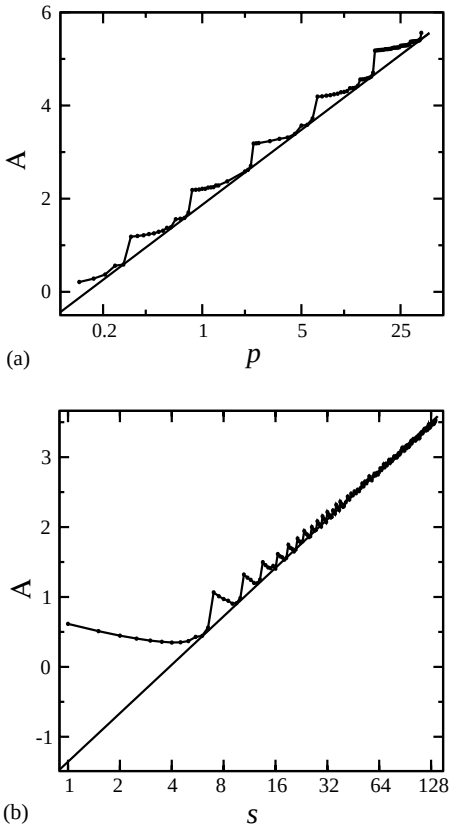

Fig. 8. Radial size of the peripheric chaotic region as a function of: (a) limiter strength; (b) magnetic shear. Full line: results from Eq. (51).

Within this predominantly chaotic region, magnetic field line diffusion is expected to yield useful information about the particle diffusion in the confined plasma [29]. We remark that this diffusion process is taken in a Lagrangian sense, and thus does not necessarily imply on a similarly chaotic diffusion of particles as time evolves. The latter problem is considerably harder to treat since it would demand a full numerical solution of the combined system of particle and electromagnetic field self-consistent equations. Field line diffusion in the outer chaotic region can be either super and sub-diffusive, characterizing an anomalous transport regime [30]. The presence of periodic islands embedded in the chaotic region influences the diffusive process. It has been investigated the connection between Tsallis non-extensive thermodynamics and anomalous diffusion [31].

From the point of view of the physical applications, the relevant diffusion in the chaotic layer near the tokamak wall is in the radial direction. It can be characterized, for example, by the evolution, with respect to the number n of complete turns around

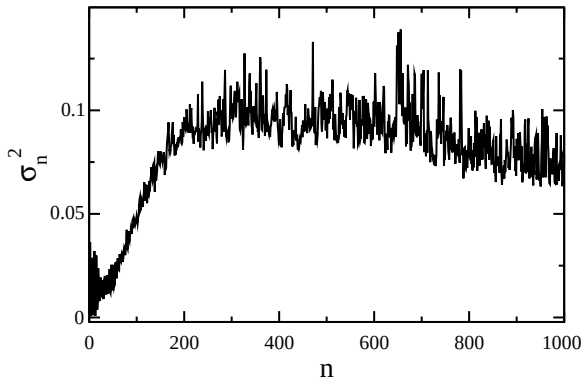

Fig. 9. Average square displacement of field lines in the radial direction versus the number of toroidal turns, for $p = 0.2$ and $s = 2\pi$, using $N_x = 10000$ initial conditions randomly chosen in the peripheric chaotic region ($y = 0.15, 0 < x < 1$).

the torus, of the average square displacement in the y-direction

$$\sigma_n^2 = \frac{1}{N_x} \sum_{i=1}^{N_x} [y_n(i) - y_0(i)]^2 \,, \tag{52}$$

where we have taken N_x initial conditions $\{y_0(1), y_0(2), \ldots\}$, randomly chosen in the chaotic region ($0 < y \lesssim A$). One expects a time evolution of this quantity in the general form $\sigma_n^2 \sim n^\nu$, where $\nu = 1$ indicates the diffusive (Gaussian) regime, and $\nu < (>) 1$ a sub-(super-)diffusive transport. Fig. 9 shows our results for the EML map (22)–(23), evidencing an initially super-diffusive regime, followed by saturation and a subsequent decay. The initially explosive phase occurs due to the dominant effect of the positive average Lyapunov exponent in the y-direction, and the observed decay is due to field line losses occurring in virtue of their collisions with the tokamaks wall at $y = 0$. This happens since points with $y < 0$ are not taken into account in Eq. (52), and after a chaotic orbit reaches $y = 0$ it escapes from the region of interest and is considered lost.

The time (in number of toroidal turns) it takes for a given field line to escape depends on the initial condition, and we analyze the average escape duration with respect to a large number of initial conditions randomly chosen in the chaotic region. We expect on general grounds an exponential distribution for the average escape time [16]. Similarly, one can compute the fraction of remaining field lines after a time n, which should also obey an exponential decay.

In Fig. 10, we plot the fraction of the remaining field lines F_p as a function of number of iterations of the EML map (22)–(23), at a fixed value of the limiter strength. For the first hundred iterations this fraction is nearly equal to unity indicating that the field lines wander through the available chaotic region practically without hitting the tokamak wall. Once this happens, however, the escape becomes very fast, occurring at an exponential rate, all field lines eventually being lost due to their colliding with the wall.

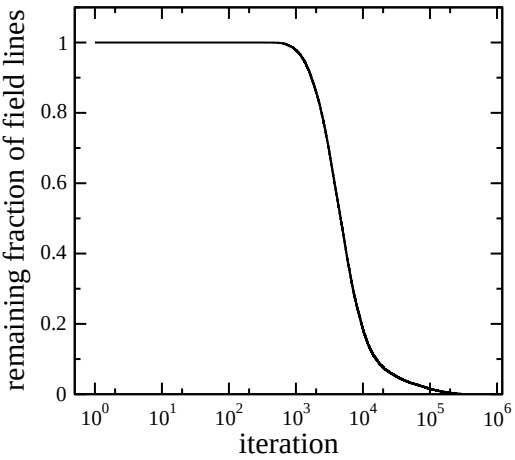

Fig. 10. Fraction of field lines which have not been lost due to collisions with the wall versus the number of toroidal turns.

Although our theoretical approach is magnetostatic, we can have a rough idea of the time it takes for a plasma ionized impurity to reach the wall. Take N randomly chosen initial conditions in the chaotic edge region (x_{0i}, y_{0i}), $i = 1, 2, \ldots, N$, and for each of them compute n_{ci}, or the number of map iterations it takes for the ith chaotic field line to reach the wall. The average number of map iterations is thus $\langle n_c \rangle = (1/N) \sum_i n_{ci}$. The escape time required for an ionized impurity to reach the wall can be thus estimated as

$$\tau_c \sim \frac{(2\pi R_0)(\langle n_c \rangle)}{v_T} , \tag{53}$$

where $v_T = \sqrt{2k_B T/m_P}$ is the particle thermal velocity, with $k_B T$ the particle thermal energy and m_P the impurity mass. This assumption underestimates effects of runaway electrons. For the tokamak *TCABR*, operating at University of Sao Paulo, it has been measured an effective atomic number of about 4.0, in such a way that we can take the berillium mass for the impurities themselves $m_P \approx 1.50 \times 10^{-26}$ kg [32]. Numerical studies of ergodic limiter performance in this machine, with a limiter current of 3.2 kA have indicated an escape time $\tau_c \approx 28$ ms, which is about one fourth of a typical discharge duration (120 ms). Hence in such a tokamak a EML can be effectively activated during plasma discharges.

Another interesting feature of the field line decay is that it is not continuous, but rather occurs in plateaus with different lengths, satisfying a well-defined statistical distribution. Fig. 11 is a frequency histogram showing the relative abundance of plateaus of given length, or the time intervals between successive losses of field lines. Here, as in the previous figure, the word time stands for the number of iterations a field line takes to hit the tokamak wall. For a given EML current we have far more small plateaus (in which field line loss occurs after a few toroidal excursions) than long plateaus.

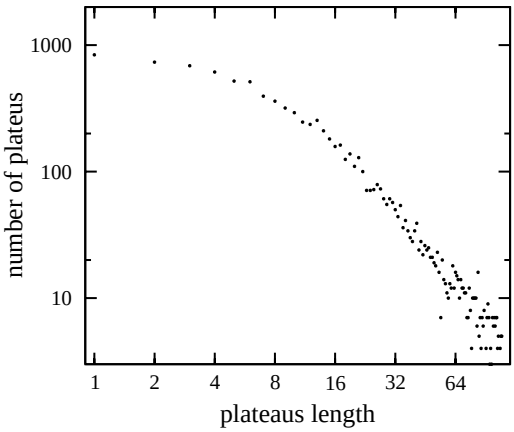

Fig. 11. Frequency histogram for the number of plateaus of a given length in Fig. 10. A plateau corresponds to the time interval between successive losses of a field line in the chaotic region.

6. Conclusions

The creation of a boundary layer of chaotic magnetic field lines is possible by means of a symmetry-breaking perturbation, and the ergodic magnetic limiter (EML) is a device with this main goal. The local character of the perturbation makes it possible to derive analytically a Poincaré map giving the field line coordinates at a fixed surface of section in the tokamak torus. In spite of the approximations which have been used to derive it, the map is rigorously area-preserving, which is a necessary requirement from the physical standpoint, and the long-term behavior of field lines can be analyzed using a considerably shorter computer time than a numerical integration of systems of differential equations.

The symplectic map we consider for the EML is such that many results have been analytically obtained in an approximate way. In this paper, we have done a careful numerical estimation of some of these approximate results. The location of the fixed points is an important information since they identify island positions and separations. We have shown that the approximate analytical expressions hold either for small limiter strength and/or high magnetic shear. The onset of global chaos, necessary to the obtention of a peripheric chaotic region, is studied by means of a modified version of the Chirikov criterion, in which touching of island separatrices is not required, and with an *ad hoc* correction being included to take care of other effects involved in the barrier transition. We have numerically determined the critical limiter current necessary to chaotization of the two outermost periodic islands and found that the value of the critical stochasticity parameter compares well with that predicted by the so-called two-thirds rule, despite the fact that the interacting islands have unequal widths.

The detailed numerical study we have done for the onset of global chaos enabled us to estimate the size of the chaotic region, by means of the average radial position of the first intact KAM surface, counted from the inner wall. Our results show a good

agreement with previous theoretical estimates. The radial diffusion of field lines in the outer chaotic region was found to be anomalous, with an initial super-diffusive regime followed by a decrease caused by losses due to field line collisions with the tokamak wall. The field line loss due to a limiter is characterized by an exponential decay, with a plateau structure when considered in smaller time scales. The plateau distribution follows a power-law dependence with the plateau duration. The symplectic map we deal with in this paper is a valuable tool to investigate the effect of symmetry-breaking perturbations on the magnetic field line structure in tokamaks, for it retains essential features also present in more sophisticated models. It is thus a useful theoretical laboratory for long-term studies of near-integrable Hamiltonian systems with a localized chaotic region.

Acknowledgements

This work was made possible through partial financial support from the following Brazilian research agencies: CNPq, Fundação Araucária (Paraná), FUNPAR (UFPR) and FAPESP (São Paulo). We acknowledge enlightening discussions and useful comments by E.C. da Silva and S.R. Lopes.

References

[1] J. Wesson, Tokamaks, Oxford University Press, Oxford, 1987.
[2] S. McCool, et al., Nucl. Fusion 29 (1989) 547.
[3] F. Karger, F. Lackner, Phys. Lett. A 61 (1977) 385.
[4] W. Engelhardt, W. Feneberg, J. Nucl. Mater. 76/77 (1978) 518.
[5] W. Feneberg, G.H. Wolf, Nucl. Fusion 27 (1981) 669.
[6] J.D. Meiss, Rev. Mod. Phys. 64 (1992) 795.
[7] P.J. Morrison, Phys. Plasma 7 (2000) 2279.
[8] A. Punjabi, H. Ali, A. Boozer, Phys. Plasma 4 (1997) 337.
[9] S.S. Abdullaev, K.H. Finken, K.H. Spatschek, Phys. Plasma 6 (1999) 153.
[10] R. Balescu, M. Vlad, F. Spineanu, Phys. Rev. E 58 (1998) 951;
R. Balescu, Phys. Rev. E 58 (1998) 3781.
[11] T.J. Martin, J.B. Taylor, Plasma Phys. Contr. Fusion 26 (1984) 321.
[12] R.L. Viana, I.L. Caldas, Z. Naturforsch. 47A (1992) 941.
[13] I.L. Caldas, J.M. Pereira, K. Ullmann, R.L. Viana, Chaos Sol. Fract. 7 (1996) 991.
[14] K. Ullmann, I.L. Caldas, Chaos Sol. Fract. 11 (2000) 2129.
[15] E.C. da Silva, I.L. Caldas, R.L. Viana, IEEE Trans. Plasma Sci. 29 (2001) 617.
[16] E.C. da Silva, I.L. Caldas, R.L. Viana, Phys. Plasma 8 (2001) 2855.
[17] E.C. da Silva, I.L. Caldas, R.L. Viana, Chaos Sol. Fract. 14 (2002) 403.
[18] E.C. da Silva, I.L. Caldas, R.L. Viana, M.A.F. Sanjuan, Escape patterns, magnetic footprints, and homoclinic tangles due to ergodic magnetic limiters, Phys. Plasmas (2002), to be published.
[19] B.V. Chirikov, Phys. Rep. 52 (1979) 265.
[20] C. Murakami, W. Murakami, Y.H. Ichikawa, Prog. Theor. Phys. 104 (2000) 723;
C. Murakami, W. Murakami, K. Hirose, Y.H. Ichikawa, Prog. Theor. Phys. 106 (2001) 909.
[21] A.J. Lichtenberg, M.A. Lieberman, Regular and Stochastic Motion, Springer, New York, Heidelberg, Berlin, 1983.
[22] R.L. Viana, I.L. Caldas, Eur. J. Phys. 12 (1991) 293.
[23] K.J. Whiteman, Rep. Prog. Phys. 40 (1977) 1033.

[24] R.L. Viana, Chaos Sol. Fract. 11 (2000) 765.
[25] R.L. Viana, D.B. Vasconcelos, Dyn. Stab. Systems 12 (1997) 75.
[26] J.M. Greene, J. Math. Phys. 20 (1979) 1183.
[27] L. Krlin, Fortschr. Phys. 37 (1989) 735.
[28] D.F. Escande, Phys. Rep. 121 (1985) 165.
[29] N. Reggiani, P.H. Sakanaka, Plasma Phys. Contr. Fusion 36 (1994) 513.
[30] V. Latora, A. Rapisarda, S. Ruffo, Physica A 280 (2000) 81.
[31] V. Latora, A. Rapisarda, C. Tsallis, Physica A 305 (2002) 129.
[32] E.C. da Silva, I.L. Caldas, R.L. Viana, Braz. J. Phys. 32 (2002) 39.